© 2019. Published by The Company of Biologists Ltd | Journal of Experimental Biology (2019) 222, jeb190983. doi:10.1242/jeb.190983

RESEARCH ARTICLE

Determinants of optimal leg use strategy: horizontal to vertical transition in the parkour wall climb

James L. Croft[1,*], Ryan T. Schroeder[2] and John E. A. Bertram[1,2,3]

ABSTRACT

This study examined the mechanics of the horizontal to vertical transition used by parkour athletes in wall climbing. We used this task as an alternative to normal running – where the functional options differ substantially – exposing the movement control priorities required to successfully complete the task. Ground reaction forces were measured in several expert parkour athletes and centre of mass trajectory was calculated from force plates embedded in the ground and the wall. Empirical measures were compared with movements predicted by a work-based control optimization model. The model captured the fundamental dynamics of the transition and therefore allowed an exploration of parameter sensitivity for success at the manoeuvre (run-up speed, foot placement, etc.). The optimal transition of both the model and the parkour athletes used a common intermediate run-up speed and appears determined largely by a trade-off between positive and negative leg work that accomplishes the task with minimum overall work.

KEY WORDS: Locomotion, Leg use, Optimization, Work

INTRODUCTION

Parkour (parcours du combattant) is a gymnastics-like athletic activity with a military–martial arts-inspired origin whose objective is to move rapidly and effectively through a complex physical environment (Atkinson, 2009; Geyh, 2006; Mould, 2009). Commonly, the complex environment of choice is an urban landscape of stairs, rails, walls and building surfaces. One common movement is landing from substantial heights (Croft and Bertram, 2017; Puddle and Maulder, 2013). Complimentary to this, these athletes must scale facades too high to simply jump (Taylor et al., 2011). For this, a distinctive running transition is often used where the legs act in a coordinated sequence, one as the last contact on the horizontal surface and the other as the initial contact on the vertical surface (Fig. 1). Owing to the aggressive nature of the perpendicular transition at speed and the elegance with which accomplished parkour athletes (traceurs) negotiate this challenge, we were interested in understanding both the physical problems involved and the solution implemented by parkour experts. We also recognized that this unusual functional circumstance could present a unique opportunity to investigate the mechanical capability and response of the legs, expecting that the specifics of the transition event may provide a novel perspective on key aspects of leg function, its limits and the factors involved in determining the movement strategy.

Ultimately, we are interested in understanding how the physiological aspects of the leg, in particular its muscular actuators and their control, interact with the Newtonian dynamics of this unconventional task. However, evaluating the control regime is particularly challenging. Certainly, it is possible to measure and describe what these athletes do while performing the task, but that gives no indication of why a particular strategy is used over other possible options. That is, simply describing the method of accomplishing the task, regardless of how meticulously, cannot distinguish the problem the movement strategy solves from the solution utilized (Croft et al., 2017).

Work-based optimization models have proved a valuable tool in understanding why certain leg use strategies are chosen in different circumstances: speed and gait (Srinivasan and Ruina, 2006), up and down slopes or stairs (Hasaneini et al., 2013), clearing obstacles (Darici et al., 2018), changes in gravitational acceleration (Polet et al., 2017), and the consequences of different functional limits and optimization goals (Srinivasan, 2011; Xiang et al., 2010). An advantage of these models is that they can generate predictive behaviours based on specific hypotheses, where the optimization cost function acts as the hypothesis describing influences that determine the best movement strategy under the imposed conditions. The hypothesis can be rigorously tested by evaluating whether the optimization model predicts key features of what humans do under those same circumstances.

In this study, we developed a simple model using a work-based energetic cost optimization as our hypothesis, then evaluated its general predictive capacity by comparing the optimal transitioning strategy it generates with that used by a group of experienced parkour athletes. The overall study proceeds in two parts: (1) evaluation of the efficacy of a work-based model for anticipating the strategy used by the parkour athletes, and (2) *post hoc* analysis of the model and the consequences of constraining key parameters (initial velocity and/or foot contact position) to understand the influences that determine movement patterns that successfully accomplish this unusual task.

MATERIALS AND METHODS

Optimization modelling

A multiphase control optimization model was developed to determine the centre of mass (CoM) trajectory that minimizes a work-based cost function. The model follows Srinivasan and Ruina (2006) and utilizes two massless legs that can extend using telescopic actuators. The leg actuators can do positive work (active extension) or negative work (resisting compression) on a point mass simulating the body mass of the parkour athlete. Although flexing knees and plantigrade feet with revolute ankle joints are not explicitly incorporated in the model, the reductionist telescopic leg

[1]Centre of Exercise and Sports Science Research, School of Medical and Health Sciences, Edith Cowan University, Perth, WA 6025, Australia. [2]Biomedical Engineering, University of Calgary, Calgary, Canada, T2N 4N1. [3]Cell Biology and Anatomy, Cumming School of Medicine, University of Calgary, Calgary, Canada, T2N 4N1.

*Author for correspondence (j.croft@ecu.edu.au)

J.L.C., 0000-0002-7457-0837

Received 20 August 2018; Accepted 5 November 2018

Journal of Experimental Biology (2019) 222, jeb190983. doi:10.1242/jeb.190983

List of abbreviations and symbols

α	angle between residual error vector and normal component of the error vector
β	complementary angle to α
θ_g	leg angle while in contact with the ground
θ_{TO}	leg angle during takeoff from the ground
BW	body weight
CoM	centre of mass (text)
$\mathbf{D}$	displacement vector between each time point of the trajectory
$\mathbf{E}_n$	normal component of trajectory's residual error
ε_1	a small number used to eliminate simultaneous positive and negative leg power
ε_2	force rate scaling constant
F_g	reaction force from the ground (model)
$\bar{F}_g$	average reaction force from the ground
$\bar{F}_w$	average reaction force from the wall
g	gravitational acceleration (9.81 m s^{-2})
GRF	ground reaction force
I_{legs}	vertical impulse of the legs
I_{vert}	vertical impulse required to climb the wall
L_{max}	maximum leg length allowed
L_g	leg length during ground contact
L_w	leg length during wall contact
J	objective function (model)
C_w	cost of leg work (model)
C_{FR}	cost of force rate (model)
L_{TD}	leg length at touchdown on the ground
L_{TO}	leg length at takeoff from the ground
m_c	centre of mass quantity
$\mathbf{p}$	body's position calculated from force plate data
$\mathbf{p}_{cam}$	body's position measured with video data
$\mathbf{p}_i$	initial body position measured with video data
RMS	root-mean-squared error
t	time (generic)
T	total transition time (horizontal to vertical)
TD	touch down of foot (initial contact)
T_g	time duration of ground contact
T_{nc}	time duration of non-contact (ballistic portions of the transition)
TO	take-off of foot (final contact)
T_w	time duration of wall contact
$\mathbf{v}$	body's velocity calculated from force plate data
$\mathbf{v}_i$	CoM velocity vector at initial contact
v_i	CoM velocity vector magnitude at initial contact
v_f	CoM velocity vector magnitude at wall grasp
W^+	quantity of positive mechanical leg work
W^-	quantity of negative mechanical leg work
x_c	horizontal position of the CoM
y_c	vertical position of the CoM
$\bar{x}_{c,g}$	average horizontal velocity of CoM during ground contact
x_{fg}	foot contact position on ground
$x_{TO,g}$	horizontal position at takeoff from the ground
y_{fw}	foot contact position on wall
$y_{c,f}$	height of the CoM at time of wall grasp
$y_{c,i}$	height of the CoM at initial ground contact
$y_{TO,w}$	height of the CoM during take-off from the wall
y_{WG}	height of the CoM at the point of wall grab

can capture much of the functional influence that these joints have on humans at a whole-body level (Lee and Farley, 1998).

In order to set boundaries on the transition from horizontal to vertical motion, a four phase optimization was implemented (Fig. 2): (i) foot contact of the last step on the ground before the wall, from touchdown (TD) to toe off (TO); (ii) no contact with either the ground or the wall; (iii) foot contact of the first step on the wall after leaving the ground; (iv) no contact with either the ground or the wall, where the CoM ballistically achieves a

Fig. 1. An example trial of a subject performing the wall climb. Centre of mass trajectory is compared as calculated from force plate data (cyan, square) and tracking a marker placed at the lower lumbar region from video (red, circle). The trajectories shown are manually adjusted to the approximate location of the greater trochanter (shift determined via visual inspection). Foot contact positions determined with centre of pressure on the force plates are shown as magenta diamonds.

height at which the top surface of the wall can be grasped. For phases (i) and (iii), only one contact leg may produce force (beginning and ending with zero force). All kinematic variables were constrained to enforce continuity between phases (i.e. final state of each phase equals initial state of the following phase). The option of simultaneous contact with both legs was not allowed at any phase; however, periods of no contact [phase (ii) and (iv)] could be near instantaneous. This was deemed reasonable since using simultaneous dual contact was not observed in any subject trials.

Initial and final conditions were prescribed to the model. Specifically, initial CoM velocity ($\mathbf{v}_i$) was constrained to reflect average run-up kinematics observed in the empirical data during part 1 of the study. Likewise, the final height and vertical velocity of the CoM were constrained in order to ensure appropriate conditions for a successful wall climb. The final horizontal position and velocity were also constrained to avoid premature collisions with the wall (in order for the optimization to conform to the task goal that the parkour athletes achieved).

Foot contact positions [x_{fg} in phase (i) and y_{fw} in phase (iii)] indicate the origin of the force vector for each leg actuator, which were constrained (in part 1 of this report, but not in part 2) by centre of pressure measurements in empirical trials. Although some subjects were observed to experience minor slipping during wall contact, we neglected this complication because of uncertainty about frictional coefficients associated with the shoe–wall interface (subjects wore their own shoes, each with slightly different friction coefficients) and complexities associated with the dynamics of a

Journal of Experimental Biology (2019) 222, jeb190983. doi:10.1242/jeb.190983

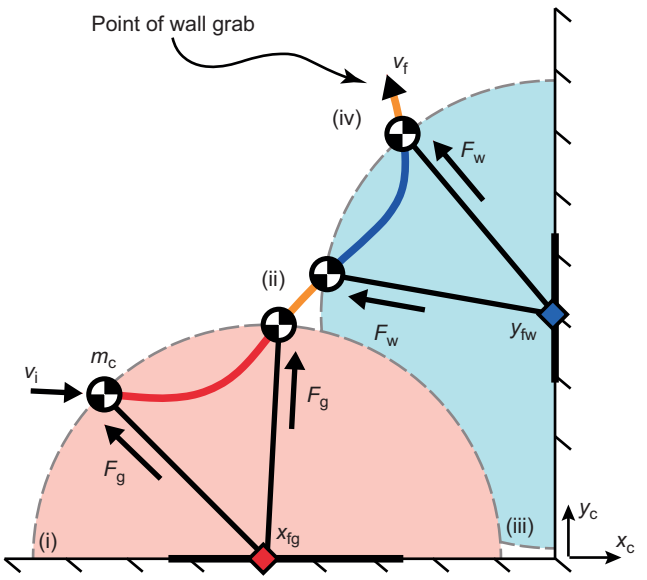

Fig. 2. Illustration of the wall climb transition from the optimization model. The four-phase optimization depicts: (i) ground foot contact, (ii) ballistic flight, (iii) wall foot contact and (iv) ballistic flight before the wall grasp (endpoint). In phases (i) and (iii), maximum leg length is enforced, and leg force is used to minimize a work-based cost and a force-rate-squared term. Empirical and optimized parameter values are compared: initial run-up velocity (v) and both foot contact positions (x_{fg} and y_{fw}). See Appendix for more details.

slip-recovery event (different slipping mechanisms can manifest in different ways and the cost of recovery likely varies accordingly). Nonetheless, slipping likely influences the required ratio of tangential to normal forces at the wall. Furthermore, there are likely realistic upper limits to force production of the legs generally. As such, upper limits to horizontal and vertical leg force components were constrained in the model to the largest forces observed from any of the experimental data. Leg length was also constrained so as not to exceed a maximum allowable leg length, as determined by averaging measurements of the distance between the ground surface and the subjects' greater trochanter (with shoes).

The cost function was determined by mechanical work performed by the leg actuators and was scaled by the efficiency of muscle contraction (25% and −120%, respectively; Margaria, 1976; Srinivasan, 2011). A force-rate-squared penalty was imposed to smooth solutions and discourage discontinuous state changes. Zero cost was implemented for non-contact phases (i.e. ballistic flight). Additional details regarding the model and its derivations can be found in the Appendix.

The control optimization evaluation was implemented in MATLAB (MathWorks) using a sparse nonlinear optimizer program (SNOPT) (Gill et al., 2005) in conjunction with GPOPS-II (Patterson and Rao, 2014) for problem discretization and setup. In order to procure robust solutions, a two-part optimization regime was employed (Schroeder and Bertram, 2018).

Despite the various constraints acting on the model in part 1 of the study (e.g. initial and final kinematic conditions, foot positions, etc.), there are a number of variables left free for the optimization to explore. Most notably, the control optimization is tasked with determining the leg force profiles that minimize work while satisfying the task constraints. Although peak forces are limited, the profile is left open for the optimization to determine. Furthermore, the model can choose to utilize leg length over any range of values that does not exceed the maximal leg length constraint. The model can also choose to modulate stance time – both at the ground and the wall – as well as flight phase times, so long as the dynamics are not violated.

Despite the solution space available in part 1, we were interested in relaxing some of the existing parameter constraints to explore a larger set of solutions. Specifically, three parameters were identified for their potential influence on an optimal transition strategy: initial CoM velocity (upon touchdown of the ground leg; v_i) and foot contact positions at the ground (x_{fg}) and wall (y_{fw}). Initially, the model was optimized with all three parameters constrained to the mean empirical values used by the subjects. This was done to test the predictive capacity of the model. Following this, these parameters were left free to be optimized over a realistic range of potential values:

$$0 \leq v_i \leq 8\ (\mathrm{m\ s^{-1}}), \quad (1)$$

$$-1.58 \leq x_{fg} \leq -0.62\ (\mathrm{m}), \quad (2)$$

$$0.72 \leq y_{fw} \leq 1.33\ (\mathrm{m}). \quad (3)$$

Bounds on foot contact positions (Eqns 2 and 3) were chosen over force plate regions, based on placement in the runway and dimensions. In part 2 of the study, multiple optimization procedures were run with the parameter v_i constrained over the range in Eqn 1 (increments of 0.5 m s^{-1}). Exploration over this range was conducted in order to more readily discern why the optimal value minimizes cost and to ultimately gain insight into the influential dynamics of the task.

Empirical measures

Participants

Seven males aged 19–33 years, height 1.72–1.90 m, leg length 0.90–1.02 m and mass 59–127 kg volunteered for this study. Peak forces from the most massive individual exceeded the reliable capacity of the force plates used in the study; subsequently, those data were excluded from analysis. Each subject had at least two years' experience in parkour and were actively training at the time of testing. Informed consent was acquired prior to testing, and all testing was performed according to a protocol approved by the local ethical review board.

Measures

A vertical wall (3.0 m height) was constructed from solid timber (90×50 mm beams) and plywood and placed in front of a custom runway (2.7 m wide; Fig. 3). Ground reaction force was measured using electronic force plates: one set into the runway and one into the wall's surface. The force plates were isolated from the runway/wall by a small gap (5 mm) and their surfaces set flush to the surrounding surface. The wall force plate was mounted to a solid frame braced directly to the reinforced cement block and steel I-beam external building wall. Placement of the ground plate was adjusted for each athlete in order to accommodate natural footfall locations determined during warm-up.

The six-axis force plates were custom designed and constructed following a standard strategy described elsewhere (Kennedy et al., 2003; Lee et al., 1999). Force plate outputs were acquired through strain conditioning amplifiers (cDAQ chassis and NI 923724-Bit Bridge Analog Input Modules, National Instruments, Austin, TX) and collected to a laptop computer via USB (2000 Hz/channel) running a custom acquisition routine written in LabVIEW (v.5.1 National Instruments). Fore–aft centre of applied pressure was calculated by calibrating the relative output of the front and rear vertical sensors (Biewener and Full, 1992). Both force plates were

Journal of Experimental Biology (2019) 222, jeb190983. doi:10.1242/jeb.190983

Fig. 3. The runway and wall constructed for this study. Two force plates are mounted independent of the plywood runway and wall to isolate them from vibrational noise, but with the top surface flush to the surrounding surface. The parkour athlete was instructed to run up and climb the wall from a starting point of their choosing.

calibrated twice a day using linear regressions to relate output signals to applied known loads. The average calibration regression parameters were used to determined force from output signals during trials.

Sagittal video was also collected (240 Hz) using an iPhone 6 (Apple Inc., Cupertino, CA) placed perpendicular to the runway at a distance of 10 m. A spherical 20 mm diameter marker was attached over the midline of the back at the level of lumbar attachment to the pelvis via a neoprene belt wrapped around the waist and pelvis. Before each subject started their trials, the video was calibrated using a 1.3×1.0 m checkerboard (100 mm squares) positioned on the ground force plate in the centre of the runway.

Procedure

Subjects were allowed to complete their own warm-up routine and were given the opportunity for practice runs to familiarize themselves with the experimental setup. When the subject indicated readiness they were instructed to run toward the wall and grasp the top surface as they would while performing parkour. They were free to start anywhere along the runway and use any preferred foot sequence on the ground and wall. Subjects were allowed to grasp the top surface of the wall in any way they desired; however, they were discouraged from using their hands on the face of the wall before reaching the top surface (since these forces would not be captured by the force plate). In the event of a hand contact during the transition, the trial was discarded. We aimed for 10 trials where the subject landed cleanly and naturally on both the ground and wall force plates. Trials were halted after 18 attempts to avoid fatigue and possible injury even if 10 useable trials had not been achieved. In total, 67 successful trials were available for analysis.

Data processing

Ground reaction force profiles

Timing of initiation and termination of foot contact – TD and TO, respectively – was determined when the force profile crossed a threshold of 3% of the subject's body weight (BW). In order to compare force profiles over multiple trials for each subject, the data from each trial were interpolated at common intervals of 0.5% of the total time duration of the force pulse. Owing to a relatively high acquisition rate of the force plate data collection (2000 Hz), the interpolation never resulted in oversampling. Mean and standard deviation were determined for each interpolation point. Time data were then re-dimensionalized to the average time duration of the pulse. This procedure was used for all force profiles. Ground and wall force profiles were then added together to characterize the entire transition and were normalized to body weight for each subject. Periods of non-contact were defined with zero force over average time durations measured from TO from the ground to TD at the wall, as well as from TO at the wall to the average time the wall was grasped. The timing of wall grasp was determined by the camera frame when a hand made contact with the top edge of the wall.

Foot contact positions

Centre of pressure profiles were calculated from the force plate data for each trial. The median value was used to characterize contact position over a given trial, rather than the mean, in order to mitigate the influence of spurious values at low force magnitudes. The median of every trial was averaged to represent foot contact for each subject. Finally, the mean and standard deviation of all subjects' centre of pressure was calculated, to characterize foot contact position on the ground and at the wall.

Video analysis

All video was exported to MATLAB for processing. A calibration factor was calculated for each subject and markers were digitized for each trial using the open source DLTdv5 package (Hedrick, 2008).

Centre of mass trajectory

The trajectory of the CoM was determined by subtracting the subject's weight from the interpolated force profile (for the vertical

Journal of Experimental Biology (2019) 222, jeb190983. doi:10.1242/jeb.190983

data) then dividing by body mass and integrating twice (for both vertical and horizontal data). Initial position of the CoM was taken from camera data. However, initial velocity was not determined by differentiating the camera data, in order to avoid differentiation noise amplification. Instead, the tracked trajectory of the lumbar marker was compared with that of the CoM trajectory from the force data with zero initial velocity and error assumed proportional to the time duration of the integration:

$$\begin{aligned}\mathbf{p}_{\text{cam}} &= \int(\mathbf{v}+\mathbf{v}_{\text{i}})dt \\ &= \mathbf{p}+\mathbf{v}_{\text{i}}t+\mathbf{p}_{\text{i}}\,,\end{aligned} \tag{4}$$

where $\mathbf{p}_{\text{cam}}$ is the tracked trajectory from the camera data, $\mathbf{p}$ and $\mathbf{v}$ are the position and velocity calculated from the force plate data integrations, $\mathbf{v}_{\text{i}}$ is the unknown initial velocity (propagating error) and $\mathbf{p}_{\text{i}}$ is the initial position taken from the camera data. A linear regression was performed on Eqn 5, where slope is the initial velocity and y-intercept is zero:

$$\mathbf{p}_{\text{cam}}-\mathbf{p}-\mathbf{p}_{\text{i}}=\mathbf{v}_{\text{i}}t\,. \tag{5}$$

Trajectories calculated from the force plate data were qualitatively compared to trajectories from the camera data to check for general agreement. Fig. 1 shows a comparison of these data for a representative trial, where changes in error likely indicate fluctuations of the true CoM as the limbs move relative to the trunk.

To calculate a representative trajectory of all the parkour athletes, each average trajectory for a subject was normalized to their individual leg length (distance measured from ground to greater trochanter). Next, the mean trajectory of all subjects was calculated and then re-dimensionalized by the average leg length of all subjects.

In order to characterize error of the intra-subject average relative to the inter-subject average, root-mean-squared error was calculated for the normal component of the residuals (Fig. 4):

$$\text{RMS}_i=\sqrt{\frac{1}{n}\sum_{j=1}^{n}\mathbf{E}_{\text{n},ij}^2}\,, \tag{6}$$

$$\mathbf{E}_{\text{n},ij}=|\mathbf{E}_{ij}|\cos(\alpha_{ij}), \tag{7}$$

$$\alpha_{ij}=90-\beta_{ij}\,, \tag{8}$$

$$\beta_{ij}=\cos^{-1}\left(\frac{\mathbf{E}_{ij}\cdot\mathbf{D}_i}{|\mathbf{E}_{ij}||\mathbf{D}_i|}\right), \tag{9}$$

$$\mathbf{E}_{ij}=\sqrt{(x_{ij}-\tilde{x}_i)^2+(y_{ij}-\tilde{y}_i)^2}, \tag{10}$$

$$\mathbf{D}_i=\sqrt{(\tilde{x}_{i+1}-\tilde{x}_i)^2+(\tilde{y}_{i+1}-\tilde{y}_i)^2}\,, \tag{11}$$

where RMS_i is the root-mean-square error of the ith data point along the trajectory, n is the number of subjects, $\mathbf{E}_{\text{n}}$ is the normal component of the error vector, α is the complementary angle to β, which is the angle between the displacement and error vectors, $\mathbf{D}$ is the displacement vector, x and y are the horizontal and vertical components of the trajectory for individual subjects and the average subject ($\tilde{x}$ and $\tilde{y}$).

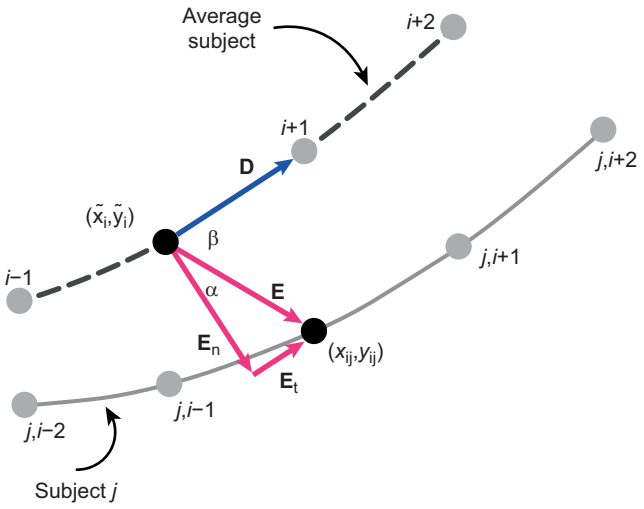

Fig. 4. Illustration of trajectory error calculation. The inter-subject average trajectory (dashed line) is compared with the intra-subject average (solid line) for the ith point and the jth subject. Root-mean-square error was calculated for the normal component of the residual vector **E**, relative to the displacement vector **D**, for all subjects (n=6) and all points along the trajectory.

RESULTS

Part 1: model compared with empirical dynamics

In Fig. 5A, the average CoM trajectory (empirical) is plotted alongside the optimization model's output. In this case, initial run-up velocity (v_{i}) and foot contact positions (x_{fg}, y_{fw}) of the model are constrained to the empirical average values. Furthermore, the CoM position at the highest point of the trajectory (when the top of the wall was grasped) is also constrained to the average for the subject trials, so the model and empirical trajectories converge toward the endpoint. Although the general curvatures of the trajectories are comparable, some differences are noted, namely during stance of the ground leg [the portion of the trajectory between the red circle (TD) and square (TO)].

The initial CoM position is higher for the empirical data than the model. This is partially due to the method used to measure leg length in our subjects. The distance from the ground to the greater trochanter while standing erect was averaged for all participants. This is likely a conservative estimate for total leg extension (as in length at TD), given that it neglects extra length available through extension at the ankle joint during plantar–flexion or tilting of the pelvis. The initial position of the empirical trajectory is derived from the camera data using a marker on the lower lumbar spine to approximate the CoM. This point on the body is higher than the greater trochanter during ground contact, and likely also contributes to the height difference observed at initial contact. We elected not to compensate for this in order to retain the simplicity of the model as much as possible without *post hoc* manipulation. Even though there were small differences between the model and the average for the parkour athletes that could have been adjusted for, we were confident the model successfully captured the main characteristics of the transition, particularly that involving the dynamics. Our primary interest was in probing the model to explore how those characteristics affected performance of the transition (part 2 of the study).

Ground reaction forces and the timing of TD and TO for both legs were also compared in the model where speed and foot position were constrained to the average used by the participants (Fig. 5C). Vertical and horizontal force profiles during contact on the ground are quite

Journal of Experimental Biology (2019) 222, jeb190983. doi:10.1242/jeb.190983

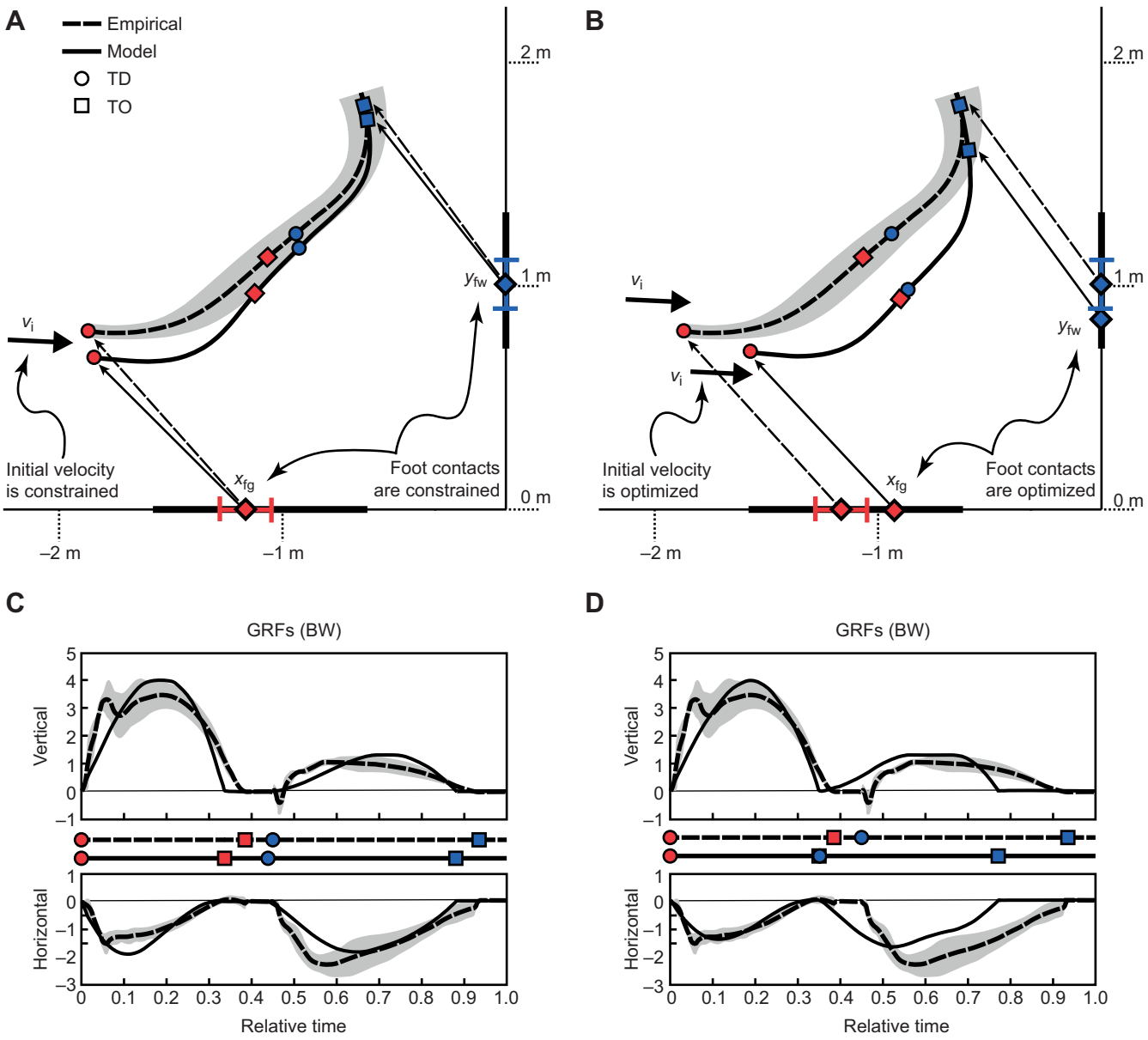

Fig. 5. Kinematics and kinetics for the optimization model and empirical data. Variables during ground contact (red) and wall contact (blue) are shown, as well as, the timing of touchdown (circle) and toe off (square). Solid line shows optimization model and dashed line is the empirical data. (A) Centre of mass trajectory and (C) ground reaction forces (GRFs) of the empirical data compared with the optimal solution where three critical parameters (initial velocity, v_i; foot contact positions, x_{fg} and y_{fw} for the ground and wall, respectively) are constrained to that of empirical values. (B) Centre of mass trajectory and (D) GRFs of the empirical data compared with the optimal solution where the three parameters are optimized in the model. Time is shown relative to final value, T_f.

similar between the empirical data and the model. The model utilizes a slightly higher magnitude, and the vertical force saturates briefly at the imposed upper limit (4 body weights; see Appendix). The empirical force rises and falls more rapidly with a slightly longer duration, which may be explained by the longer functional leg length in the subjects (the leg can extend for a longer period of time before TO). Another difference is the presence of an impact spike in empirical force at initial ground contact. This spike is typical of running gaits, where the mass of the leg is decelerated prior to the rest of the body (Bobbert et al., 1992; Liu and Nigg, 2000). Since the model has massless legs, this initial force spike is not present.

A much smaller initial force peak is seen when contact is made with the wall. In this case, contact is initiated just after the body rises during the brief non-contact, ballistic phase. This results in the initial vertical force application being negative, where the foot is abruptly brought to a stop at contact. The remainder of the wall force profile is similar between the model and the subject average, although the peak tends to occur somewhat earlier in the empirical data. Wall contact is slightly longer for the subject average. This may be partially explained by the subject's additional functional leg length or else the magnitude of the force rate scaling constant (ε_2) used in the model.

A comparison similar to that above, but where the three parameters are left open for optimization (initial velocity and foot position on the ground and the wall) is shown in Fig. 5B,D. The initial velocity of the model is less than a standard deviation from the participant average (4.49 vs 4.70±0.40 m s^{-1}). In contrast, the foot contact positions are both shifted away from the empirical average (−0.99 vs −1.17 for x_{fg}; 0.88 vs 1.01 m for y_{fw}) where both occur closer to the ground–wall interface in the model optimizations.

Journal of Experimental Biology (2019) 222, jeb190983. doi:10.1242/jeb.190983

Although the general shape of the trajectory is not much affected, one key difference is that non-contact ballistic flight between the ground and wall contacts (phase ii) is largely eliminated. Since foot contact position at the wall is lower, the CoM at TO from the wall is also lower (i.e. leg geometry is mostly conserved). Subsequently, the time of TO from the wall occurs much earlier in the model and flight duration after leaving the wall is extended before the wall grasp is achieved.

Leg force saturation occurs in both model conditions (constrained and unconstrained) but to different extents. In the unconstrained model, vertical force peaks saturate the upper bound for both legs, although only briefly for the ground contact leg. In contrast, horizontal ground reaction force peaks appear to be less constrained by these bounds. In all cases of force saturation, the saturation occurs for minor to moderate durations, and as such, the bounds do not overly influence the optimal solutions. The longest duration of force saturation occurs for vertical force of the wall contact leg in the unconstrained model, indicating that the model would likely choose higher force magnitudes if the force bound were left unconstrained. It is possible that human subjects did not display higher forces to mitigate slipping at the wall. This was not included in the model as we elected to leave the model as simple as possible so that factors determining the results could be clearly interpreted.

A distinctively horizontal TD trajectory entering the beginning of the transition is used by both the model and the participants, and is followed by a much steeper angle at TO from the ground. This asymmetrical trajectory has been observed in individuals jumping over obstacles during running (Mauroy et al., 2013). Also common between the model and participants is the use of a leg angle above horizontal at wall contact. This angle likely helps reduce negative leg work during this phase of the transition (and momentum loss), since force angle is defined by the leg's orientation.

Part 2: model sensitivity to parameter constraints

Consequences of initial velocity on cost and transition strategy

Net leg work for the parkour wall climb is minimized (in fact, zero) when the kinetic energy associated with initial velocity is equal to the final kinetic energy plus the potential energy required for height change from initial ground contact to the point of wall grasp.

$$\frac{1}{2}m_c v_i^2 = \frac{1}{2}m_c v_f^2 + m_c g(y_{c,f} - y_{c,i}), \quad (12)$$

$$v_i = \sqrt{v_f^2 + 2g(y_{c,f} - y_{c,i})}, \quad (13)$$

where m_c is the total body mass, v_i is the body's velocity at initial ground contact, v_f is the body's velocity at wall grasp, g is gravitational acceleration (9.81 m s^{-2}), $y_{c,f}$ is the body's height at the time of the wall grasp and $y_{c,i}$ is the body's height when the ground leg initiates contact. Note that zero net leg work means whatever positive work is done by the legs is equal to, and therefore cancels out, the negative work performed by the legs.

It is perhaps unsurprising that the average initial velocity of the empirical trials is less than a standard deviation from the initial velocity calculated for zero net leg work (4.70±0.40 vs 4.78 m s^{-1}, respectively). A higher initial velocity requires more negative work throughout the transition and a lower initial velocity requires more positive work (i.e. increased cost; Fig. 6A). However, when the initial velocity is optimized as a free parameter (between 0.5 and 8.0 m s^{-1}), the model chooses a slower initial velocity (4.49 m s^{-1}) that requires additional positive work to manage the transition.

Although net leg work – as a metric for energy consumption – represents the minimum the legs must do in order to manage a successful transition, it obscures the total work done by the legs, since positive work can cancel negative work during summation. For example, during the step-to-step transition in walking, positive work due to push off of the trailing limb occurs simultaneously with negative work of the leading limb performing heel strike, and this imparts a substantial cost for walking (Donelan et al., 2002a,b), even though the net work of a steady state gait is necessarily zero. Although our model cannot use simultaneous contact of both limbs, there is substantial positive and negative work done over the transition from horizontal to vertical.

To fully account for this work, we evaluate the absolute value of the work performed by the legs (Fig. 6A). At an initial velocity of 5 m s^{-1} (approximately zero net leg work), the absolute work performed is non-zero and moreover, the minimum value does not occur at this speed. Instead, it is found at a speed of 3 m s^{-1}, where virtually all work is positive. Interestingly, absolute leg work approaches minimum net leg work at lower initial velocities, but it is much larger at higher initial velocities (Fig. 6A). When absolute work is scaled by the inverse of muscle efficiency (25% and −120% for positive and negative work, respectively), the minimum cost solution is found near an initial velocity associated with zero net leg work. The muscle efficiency scaling makes positive work four times more expensive while simultaneously reducing the cost of negative work by almost 17%. Since the optimal solution before scaling is dominated by positive leg work, it becomes a much more costly option. Instead, the minimum cost solution occurs at a faster run-up velocity where net leg work happens to be approximately zero. However, there does not appear to be any obvious functional meaning to the alignment with zero net leg work, beyond that of the cost rescaling for positive and negative work.

In order to understand why absolute leg work approaches net leg work at lower speeds but is much costlier at higher speeds, individual leg work is indicated over the same range of speeds (Fig. 6B). The height of the curve above zero indicates positive work and height below zero indicates negative work for the ground leg (red) and the wall leg (blue). The region between these limits is filled simply in order to assist the reader in evaluating the relative change in each as the vertical range of the shape indicates absolute work of the leg at any given speed. Furthermore, the model metrics are compared with that of the empirical data, albeit only for the average initial velocity that the subjects selected themselves (Fig. 6B). In general, the model tends to over-predict leg work; however, the approximate proportions of positive and negative work per leg are comparable. Specifically, the average subject's non-dimensional positive and negative work of the ground leg are 0.47 and −0.34 (versus 0.60 and −0.52 predicted by the model at the same speed). Similarly, the average subject's non-dimensional positive and negative work of the wall leg are 0.17 and −0.30 (versus 0.23 and −0.16 predicted by the model at the same speed). Note that the data point for negative work of the wall leg is nearly coincident with the data point for negative work of the ground leg which tends to obscure the point (marked with an asterisk in Fig. 6B).

It seems reasonable that negative work approaches zero at lower speeds since little momentum is available and net positive work is required to achieve the required height change. Yet at the highest speeds (where net negative work is required) positive work still increases substantially for the ground leg and negative work is exaggerated in both legs to compensate. This apparent wastefulness suggests limited strategies are available to the model at these speeds, since only optimal solutions for each defined circumstance are displayed (e.g. the output of the optimization model).

Journal of Experimental Biology (2019) 222, jeb190983. doi:10.1242/jeb.190983

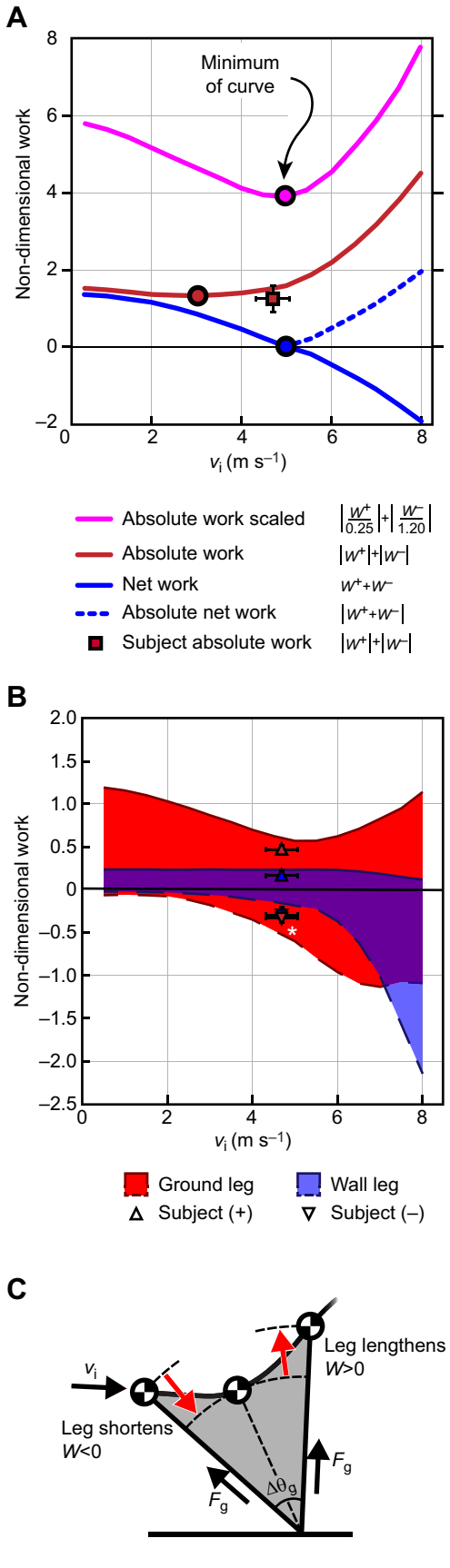

Fig. 6. Work cost of parkour wall climbing optimization model over a range of initial velocities. (A) The cost function utilized for the optimizations is shown (magenta) where the absolute value of positive and negative work is scaled by the efficiency of muscle: 25% and −120%, respectively. The absolute value of work is also shown without scaling (dark red), as well as the average absolute work calculated from empirical data (dark red square) and standard deviation (error bars). Finally, net work is shown (blue) and the absolute value of net work is indicated by the dashed line. The black circle indicates the minimum of each work curve. (B) Work is shown for the leg in contact with the ground (red) as well as the leg in contact with the wall (blue). The height of the shape above zero indicates the magnitude of positive work (solid line) while the height of the shape below zero indicates the magnitude of negative work (dashed line) for the associated leg. As such, the total height of the shape (top minus bottom) is proportional to the total absolute work done by the associated leg at any given initial velocity. Average empirical values and their standard deviation are provided for comparison with the model (symbols identified in the legend). Note that the negative work value for the wall leg is nearly coincident with that of the ground leg, so the ground leg symbol obscures that of the wall leg (white asterisk). (C) Diagram showing the relationship of leg angle geometry to mechanical work; the leg actively resists compression towards the first half of stance (negative work) and extends toward the second half of stance (positive work).

Leg work is performed by the ground leg as it actively resists compression toward the beginning of stance (negative work) and extends toward the end of stance (positive work; Fig. 6C). Why should the leg extend more at higher speeds, if net negative work is needed? One requirement of the model is that the legs must provide enough vertical impulse to manage the transition. The vertical impulse must overcome the force of body weight during the transition and redirect momentum from downward (prior to initial contact) to upward (at the wall grasp) (Eqn 14). The required vertical impulse I_{vert} is calculated as:

$$I_{vert} = -m_c g T + m_c(\dot{y}_{c,f} - \dot{y}_{c,i}), \quad (14)$$

where T is the total time duration of the wall climb transition, $\dot{y}_{c,f}$ is the final vertical velocity and $\dot{y}_{c,i}$ is the initial vertical velocity (recall, these variables are model inputs, as determined from the empirical trials).

The vertical impulse of the legs is defined by the integral of vertical leg force during contact and can be characterized by the product of two parameters (per leg): average vertical force and time of contact (Eqn 15),

$$I_{legs} = \tilde{F}_g T_g + \tilde{F}_w T_w, \quad (15)$$

where I_{legs} is the vertical impulse of the legs (I_{legs}=I_{vert}), $\tilde{F}$ and T are the average vertical force and the time duration of contact, respectively, for the ground ($\tilde{F}_g$, T_g) and wall ($\tilde{F}_w$, T_w) legs.

At higher initial speeds, achieving the required vertical impulse is likely more difficult since the body travels over the leg more quickly, and this leaves less time to provide upward force. Fig. 7A,B shows that the angular displacement of the leg during ground contact increases substantially at higher initial velocities, and this strategy may allow more contact time in order to manage the required vertical impulse. Specifically, the time of contact is related to the leg's angular displacement ($\Delta\theta_g$) via Eqns 16 and 17 (Fig. 7B):

$$T_g = \frac{\Delta x_c}{\tilde{\dot{x}}_{c,g}}, \quad (16)$$

$$\Delta x_c = L_{TO}\cos(\theta_{TO}) - L_{TD}\cos(\Delta\theta_g + \theta_{TO}), \quad (17)$$

where $\tilde{\dot{x}}_{c,g}$ and Δx_c are the average horizontal velocity and the horizontal displacement of the CoM over stance of the ground leg respectively, L and θ are the length and angle of the ground leg at toe off (TO, contact termination) and touchdown (TD, initial contact).

Journal of Experimental Biology (2019) 222, jeb190983. doi:10.1242/jeb.190983

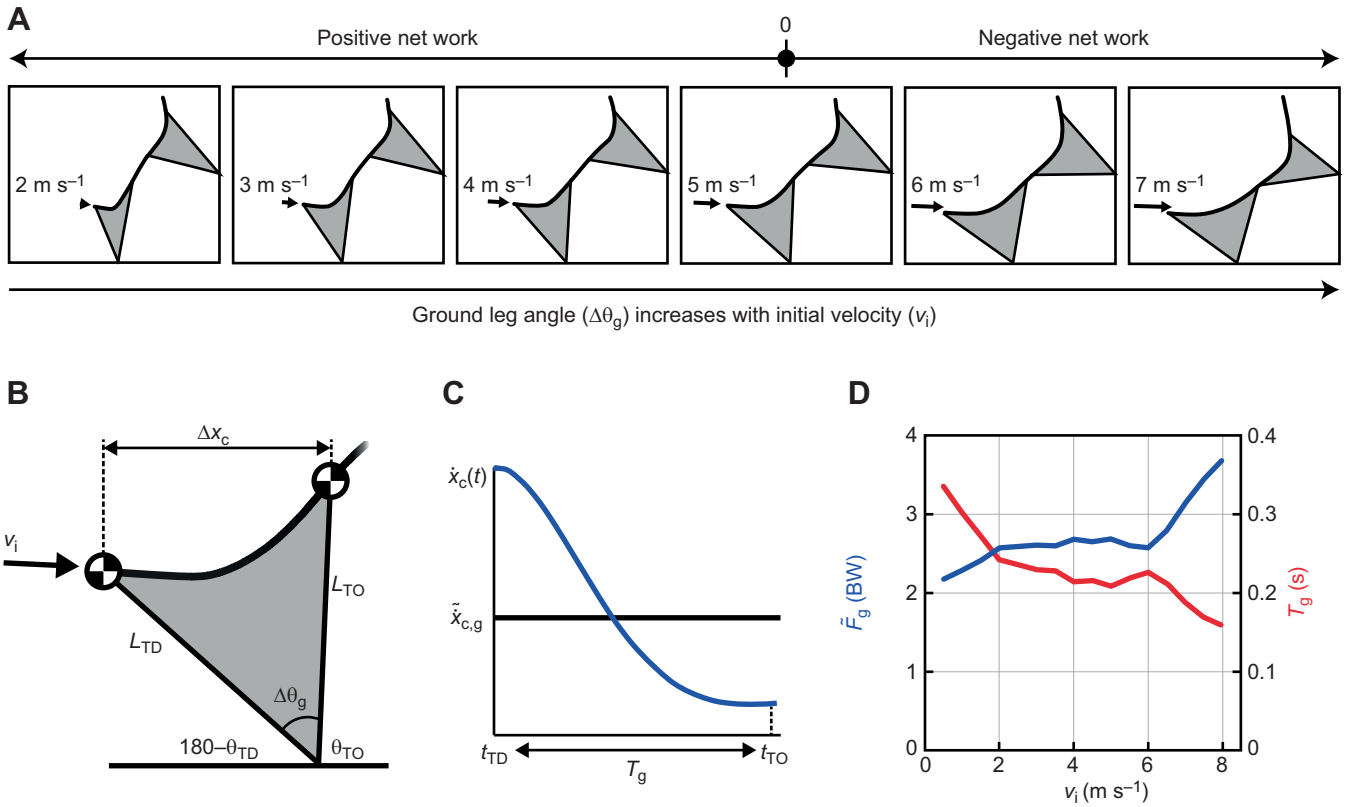

Fig. 7. Angular displacement of the leg in the optimization model increases to help provide necessary vertical impulse during stance. (A) Centre of mass trajectory over a range of initial velocities. The angular displacement of the ground contact leg increases with initial velocity. (B) Diagram showing the relationship of leg angle range to time of ground contact during stance; time duration equals horizontal displacement divided by average horizontal velocity. (C) Horizontal velocity decreases over stance of the leg in contact with the ground. Initial velocity condition shifts the average horizontal velocity up or down and leg compliance determines the magnitude of the decrease over stance. (D) The two components of vertical impulse – average leg force and time of contact – are shown for the ground leg over a range of initial velocities. Although increased leg angles help to provide more time of contact, the contact period still decreases, and the average force increases at higher initial velocities (approaches force saturation via the leg force constraint in the model: 4 BW).

Since $\tilde{\dot{x}}_{c,g}$ is shifted by the initial velocity and scaled by the general compliance of the leg (Fig. 7C), an increase in $\tilde{\dot{x}}_{c,g}$ due to higher initial velocity can be counteracted by an increase in the leg's angular displacement and a subsequent increase in Δx_c. It is also possible to simply increase average leg force to counteract a shorter contact time and maintain the necessary vertical impulse. However, vertical leg force is constrained (limit set at the upper range of the force data from the empirical study: 4 BW for the ground leg). If the upper bound on vertical leg force is saturated, then the average vertical force can only be increased with higher force rates, which are cost-penalized by the model. Furthermore, larger force magnitudes generally increase leg work, since mechanical power is proportional to force magnitude. In reality, an optimal combination of these strategies is used over the range of initial velocities. The leg's angular displacement increases, and this likely mitigates a reduction in stance time due to higher velocity, yet stance time still decreases with higher initial velocities overall (Fig. 7D). As such, average vertical leg force increases to compensate. It is likely that this interaction incurs a larger work cost at higher initial velocities and requires the leg to produce unnecessary positive work as a means to mitigate reductions in stance time.

Consequences of foot contact position on cost and transition strategy

The previous section describes how the vertical impulse of the legs can be modulated (average force, time of contact) in order to optimally manage the wall climb transition over a range of initial speeds. However, it is also possible to reduce the vertical impulse required (I_{vert}, Eqn 14). Although the change in momentum is predetermined by the empirical data, the total time duration of the transition may be reduced. Total time duration is given by the sum of times of contact (for both ground and wall legs) plus time of non-contact (i.e. flight phase):

$$T = T_g + T_w + T_{nc}, \quad (18)$$

$$T_{nc} = T_{nc1} + T_{nc2}, \quad (19)$$

where T_{nc1} is the time of non-contact between ground contact and wall contact and T_{nc2} is the time of non-contact between wall contact and wall grasp. Although reducing T_g or T_w may reduce the necessary impulse, it also reduces the impulse provided by the legs, which is counterproductive. However, if it is possible to reduce the time of non-contact (T_{nc}), then this could potentially reduce the impulse required without affecting the impulse provided by the legs. One such strategy is to choose foot contact locations that allow for the time of non-contact between the ground and the wall to approach zero (Fig. 5B). That is, the support leg shifts from the ground to the wall without an intervening flight phase. Owing to the maximum leg length constraint, foot contact positions must be chosen such that the optimal leg length/angle on the ground aligns the body with the optimal leg length/angle on the wall, and this requires both contact positions to be closer to the wall–ground interface. The model converges on this solution when foot contact positions are

Journal of Experimental Biology (2019) 222, jeb190983. doi:10.1242/jeb.190983

optimized within a range defined by the force plate surface: ground foot contact is −0.99 m and wall foot contact is 0.88 m (Fig. 5B).

Still, by lowering the foot contact on the wall, this also lowers the height of the CoM as it leaves contact with the wall, and this could potentially increase T_{nc2}. The flight time is described by kinematic relationships, assuming that gravity is the only force acting on the body. When foot contact positions are constrained to those seen empirically, the flight time is described by Eqn 20:

$$T_{nc,emp} = \frac{\Delta x_{nc1}}{\dot{x}_{TO,g}} + \frac{2(y_{WG} - y_{TO,w})}{\dot{y}_{WG} + \dot{y}_{TO,w}}, \quad (20)$$

where Δx_{nc1} is the horizontal displacement of the CoM during the non-contact phase between ground and wall contact, $\dot{x}_{TO,g}$ is the horizontal velocity of the CoM at toe-off from the ground, y and $\dot{y}$ are the CoM vertical position and velocity at the wall grab (WG) and at toe-off from the wall (TO,w).

When foot contact positions are left free to be optimized, T_{nc1} equals zero, but the CoM leaves the wall contact from a lower height ($y_{TO,w}$ is lower than in Eqn 20):

$$T_{nc,opt} = \frac{2(y_{WG} - y_{TO,w})}{\dot{y}_{WG} + \dot{y}_{TO,w}}. \quad (21)$$

If $T_{nc,emp} > T_{nc,opt}$, then the required impulse is lower when foot contacts are closer to the ground–wall interface. Indeed, when foot contact positions are optimized, the time of non-contact is decreased by 10% (from 0.140 to 0.126 s) and average vertical force of the ground leg is also decreased by about 3% (from 2.67 to 2.59 BW). Ultimately, allowing the foot contact placements to be optimized allows for the non-dimensional work-based cost of the solution to be reduced by about 4.1% (from 3.92 to 3.76).

Given the potential cost savings of using foot contacts closer to the ground–wall interface, it is fair to ask why the parkour athletes used such a large flight phase between the ground and wall contacts. One potential explanation is that there is an additional cost, which the model does not take into account: that of leg swing. With less non-contact time between the ground and wall contacts, there is less time for the leg to swing through to the next contact. Given that the work to swing a pendular leg increases with frequency (Doke et al., 2005; Polet et al., 2017; Srinivasan, 2011), this extra cost may help explain why the parkour athletes did not utilize this strategy. This issue is not considered in our model because it has massless legs. More sophisticated human models could incorporate legs with appropriate mass in order to determine if leg swing cost influences the optimal transition dynamics for the parkour wall climb.

DISCUSSION

The objective of this study was to gain insight into the factors that influence leg use strategy in locomotion. Although the brain is ultimately in control, to successfully accomplish a locomotory task, the strategy employed must integrate the physiological capabilities (constraints and opportunities) within the dynamic, physical affordances available. For a complex task such as the parkour wall run, however, it is difficult to distinguish physiological and physical opportunities and limitations. Our approach was to investigate the physical factors using a simple, work-based optimization model, and then compare resulting solutions to the strategy used by experienced parkour athletes. We chose the parkour wall run because it has distinctive differences from standard locomotion while still utilizing the same machinery (the legs). We expected that this would contrast the influence of physical and physiological aspects of the manoeuvre by highlighting differences between the model and human behaviour. Presumably, these differences are largely influenced by physiological/morphological distinctions between the model and the human system and thus, provide unique insight into factors that are utilized to successfully accomplish this demanding locomotor task.

The study proceeded in two parts. First, a simple work-based model anticipating an optimal running transition from a horizontal to a vertical surface contact was compared to a group of expert parkour athletes performing the parkour wall run, a manoeuvre designed to allow an individual to scale a wall too high to simply leap. The objective of the modelling exercise was not to reproduce the floor to wall transition with high fidelity, but to generate a model that captured the key dynamic factors that contribute to a successful transition. Initial validation of the basic model was followed by an exploration of specific parameter constraints. This was done to gain insight into the influences that determine the optimal transition strategy. In order to place these results in context, substantial discussion and interpretation has been integrated into the results narrative.

One notable difference between the model and the human is the angle of leg forces at some points in the transition. The model utilizes an actuator that can only apply force along the axis of the leg, whereas the multi-jointed human leg can deviate from this physical constraint through applying torques, for instance at the hip. Although the simple leg actuator is successful at capturing much of the empirical transition dynamics, there are differences between the model and empirical force orientations. Specifically, notable differences were observed for subjects toward the end of contact with the wall, where the human force angle became substantially more horizontal than the leg angle (Fig. 8). It should be noted that the data in Fig. 8 was chosen to illustrate one of the more pronounced examples of this effect, although it was not an isolated case. It may be that deviations like this function to increase the ratio of normal force to tangential force in order to increase friction and reduce slipping at the wall. Other deviations are observed in Fig. 8 toward the beginning of each stance phase. These periods of transient deviation are likely due to leg retraction, where the leg pulls back just before contact. Deviations such as these can help

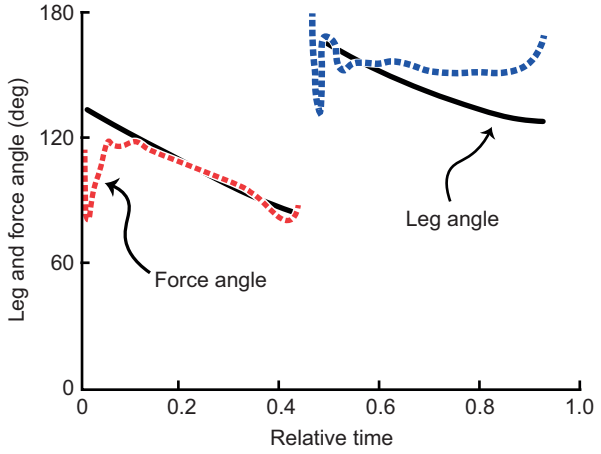

Fig. 8. Vector angles for leg force and position are shown for an example subject. Zero degrees is defined horizontal pointing to the right and positive is counter-clockwise. The solid black lines indicate changes in leg angle over time (shown relative to final value, T_f) and the dashed lines indicate the angle of the corresponding force vector. Red signifies contact at the ground and blue for contact at the wall. Note that these two angles are perfectly coincident in the model. However, notable deviations occur in human data.

smoothen out the transition from horizontal to vertical and mitigate energy loss due to collision-like contacts. We chose not to incorporate more complicated leg actuation in order to maintain simplicity of the model. However, future more-complex versions could certainly explore additions such as actuation at the hip, in order to come closer to the empirical solutions presented here.

Balancing work and impulse to optimize the horizontal to vertical transition

An important value of the work optimization model is that its outputs can be dissected in order to probe why optimal strategies are indeed optimal. We tested a range of parameters (initial run-up velocity and foot contact positions) and derived positive and negative work relationships contributing to the overall cost and strategy utilized to accomplish the task (Fig. 6).

At slow initial velocities, the individual has only modest horizontal momentum (and no vertical momentum) so the task goal (reaching the determined height) is achieved almost exclusively with positive work. This is not a bad strategy since the relatively low speed allows for more contact time to provide enough force to generate the necessary impulse.

The amount of positive work required decreases as speed is increased. This is because horizontal momentum can be partially redirected to vertical momentum with a strut-like leg. At very high speeds, the excess momentum is absorbed with negative work, and this occurs particularly by the leg contacting the wall. However, substantial positive work is also necessary on the floor in order to produce the required vertical impulse, though appropriate placement of foot contacts can help alleviate some of this cost. Although high positive work dominates at slow run-up speeds (2 m s^{-1}) and high negative work is required at high run-up speeds (8 m s^{-1}), minimal absolute work occurs at a relatively low speed (3 m s^{-1}). However, the scaling of muscle efficiency for negative work means that the physiological optimum is shifted back toward an intermediate speed (5 m s^{-1}), quite close to the average speed used by the parkour athletes (Fig. 6A).

We elected to explore a model with actuated legs that can do positive and negative leg work on the CoM. Alternatively, the transition could have been viewed from the perspective of collision losses and the leg work needed to replace those losses (Ruina et al., 2005). In theory, it would not be necessary to do any work with the legs if there were no collision losses involved and assuming a sufficient starting energy. In dynamics, a collision is simply a discontinuity of the CoM velocity vector caused by an applied force. This will inevitably involve energy loss unless the applied force is perpendicular to the instantaneous CoM velocity vector. The perfect transition, then, could involve a force continuously applied at right angles to the CoM velocity vector over the course of the transition, as could be accomplished with a frictionless curved ramp or an infinite number of legs, each with the appropriate leg angle. For this situation, the optimal approach speed would be that with precisely the kinetic energy to allow conversion to the required potential energy to accomplish the task. Given that the human has just two legs, it is impossible to achieve this ideal. The value of the analysis presented here is to place the leg use strategy in the context of the opportunities and trade-offs available.

The parkour wall run is an unusual manoeuvre with similarities to and differences from overground locomotion. In this study, we showed that a substantial portion of the leg use strategy can be captured using a relatively simple work minimization model. Employing this model allowed a convenient exploration of the factors that contribute to the optimization, which in turn provides insight into why the particular leg use strategy is implemented by experienced athletes executing an unusual and challenging physical manoeuvre.

Appendix

The four-phase optimization model allows the telescopic legs to perform work on the centre of mass depending on the phase. Only one leg can provide force to the point mass body at a time during phases (i) and (iii) at the ground and wall surfaces, respectively. During phases (ii) and (iv), only gravitational forces are felt by the point mass. These dynamics are defined mathematically in Eqn A1:

$$\begin{bmatrix} \ddot{x}_c\,(\mathrm{i}) \\ \ddot{y}_c\,(\mathrm{i}) \\ \ddot{x}_c\,(\mathrm{ii}) \\ \ddot{y}_c\,(\mathrm{ii}) \\ \ddot{x}_c\,(\mathrm{iii}) \\ \ddot{y}_c\,(\mathrm{iii}) \\ \ddot{x}_c\,(\mathrm{iv}) \\ \ddot{y}_c\,(\mathrm{iv}) \end{bmatrix} = \frac{1}{m_c} \begin{bmatrix} F_g\left(\frac{x_c - x_{fg}}{L_g}\right) \\ F_g\left(\frac{y_c}{L_g}\right) - m_c g \\ 0 \\ -m_c g \\ F_w\left(\frac{x_c}{L_w}\right) \\ F_w\left(\frac{y_c - y_{fw}}{L_w}\right) - m_c g \\ 0 \\ -m_c g \end{bmatrix}, \tag{A1}$$

where x_c and y_c are the horizontal and vertical kinematics of the centre of mass (CoM), respectively, for phases (i) through (iv). **F** is the force of the leg actuator in contact with the ground [F_g; phase (i)] and the wall [F_w; phase (iii)], x_{fg} and y_{fw} are the horizontal and vertical foot contact positions of the ground and wall legs, respectively, m_c is the CoM and $\boldsymbol{g}$ is the gravitational acceleration constant (9.81 m s^{-1}).

Leg length and velocity are defined for both legs in Eqns A2–A5.

$$L_g = \sqrt{(x_c - x_{fg})^2 + y_c^2}, \tag{A2}$$

$$\dot{L}_g = \frac{(x_c - x_{fg})\dot{x}_c + y_c\dot{y}_c}{L_g}, \tag{A3}$$

$$L_w = \sqrt{x_c^2 + (y_c - y_{fw})^2}, \tag{A4}$$

$$\dot{L}_w = \frac{x_c\dot{x}_c + (y_c - y_{fw})\dot{y}_c}{L_w}. \tag{A5}$$

Given the intense physicality required by the wall climb manoeuvre, it is likely that athletes may be limited by their physical capabilities. As such, upper limits to horizontal and vertical leg force components were constrained in the model to the largest forces observed from all the experimental data (normalized by body weight). In the case of force components normal to the substrate surface, only forces in the direction away from the surface were allowed [positive in phase (i), negative in phase (iii)]. In the case of tangential forces, the largest force value (whether positive or

negative) was used for the constraint in both directions:

$$-2.5 \leq \frac{F_{g,x}}{m_c g} \leq 2.5\,, \tag{A6}$$

$$0 \leq \frac{F_{g,y}}{m_c g} \leq 4.0\,, \tag{A7}$$

$$-12.6 \leq \frac{F_{w,x}}{m_c g} \leq 0\,, \tag{A8}$$

$$-1.3 \leq \frac{F_{w,y}}{m_c g} \leq 1.3\,. \tag{A9}$$

Leg length was also constrained so as not to exceed a maximum allowable leg length, as determined by averaging measurements of the distance between the ground surface and the subjects' greater trochanter (with shoes):

$$L_{max} - L_g \geq 0, \tag{A10}$$

$$L_{max} - L_w \geq 0\,. \tag{A11}$$

A work-based cost function (C_w) was used to implement the control optimization protocol for phases (i) and (iii). A force-rate-squared cost (C_{FR}) was also implemented in order to smooth solutions and discourage discontinuous state changes. Zero cost was implemented for phases (ii) and (iv) (non-contact, i.e. ballistic flight):

$$J = \sum_{i=1}^{n=4} J\,(\mathrm{i}), \tag{A12}$$

$$\begin{bmatrix} J\,(\mathrm{i}) \\ J\,(\mathrm{ii}) \\ J\,(\mathrm{iii}) \\ J\,(\mathrm{iv}) \end{bmatrix} = \int_{t_i}^{t_f} \begin{bmatrix} C_w + C_{FR} \\ 0 \\ C_w + C_{FR} \\ 0 \end{bmatrix} dt\,. \tag{A13}$$

The work-based cost function scaled positive and negative mechanical power of the legs by muscle efficiency associated with concentric and eccentric contraction [25% and −120%, respectively (Margaria, 1976; Srinivasan, 2011)]:

$$C_w = \frac{\dot{W}^+}{0.25} + \frac{\dot{W}^-}{-1.20}\,, \tag{A14}$$

$$\dot{W} = F\dot{L} = \dot{W}^+ - \dot{W}^-\,, \tag{A15}$$

where $\dot{W}$, $\mathbf{F}$ and $\dot{L}$ are the mechanical power, force, and contraction velocity of the leg actuators, respectively. Orthogonality of $\dot{W}^+$ and $\dot{W}^-$ was ensured by introducing an additional term to the cost function for phases (i) and (iii): $\epsilon_1 \dot{W}^+ \dot{W}^-$. In all optimizations, this term was driven to zero (no contribution to overall cost); however, it prevents the leg actuators from producing positive and negative work simultaneously. The force-rate-squared cost term is defined in Eqn A16:

$$C_{FR} = \epsilon_2 \dot{F}^2\,, \tag{A16}$$

where ϵ_2 is a small number that scales the force-rate-squared cost.

The control optimization procedure was implemented in MATLAB using a sparse nonlinear optimizer program (SNOPT) (Gill et al., 2005) in conjunction with GPOPS-II (Patterson and Rao, 2014) for problem discretization and setup. In order to procure robust solutions, a two-part optimization regime was used (Schroeder and Bertram, 2018). The first part implemented 15 random initial guesses to test for global optimality, and the second perturbed the prevailing optimum 15 times with random noise in order to fine tune the solution's local optimality.

The optimization procedure was performed for various parameter constraints. Specifically, three parameters were identified for their potential influence on an optimal transition strategy: initial CoM velocity (upon touchdown of the ground leg; v_i) and foot contact positions at the ground (x_{fg}) and wall (y_{fw}). In part 1 of the study, the model was optimized with all three parameters constrained to the empirical data of subjects to test the predictive capacity of the model. Next, they were left free to be optimized over a realistic range of potential values:

$$0 \leq v_i \leq 8\ (\mathrm{m\ s^{-1}}), \tag{A17}$$

$$-1.58 \leq x_{fg} \leq -0.62\ (\mathrm{m}), \tag{A18}$$

$$0.72 \leq y_{fw} \leq 1.33\ (m). \tag{A19}$$

Acknowledgements
We would like to thank the members of Perth Parkour Association who volunteered their time and considerable skill to make this study possible.

Competing interests
The authors declare no competing or financial interests.

Author contributions
Conceptualization: J.L.C., J.E.B.; Methodology: J.L.C., R.T.S., J.E.B.; Formal analysis: R.T.S.; Investigation: J.L.C., R.T.S., J.E.B.; Writing - original draft: R.T.S., J.E.B.; Writing - review & editing: J.L.C., R.T.S., J.E.B.; Supervision: J.L.C., J.E.B.; Project administration: J.L.C.

Funding
This study was funded by an NSERC (Canada) Discovery grant (04823-2017 to J.E.A.B.).

References

Atkinson, M. (2009). Parkour, anarcho-environmentalism, and poiesis. *J. Sport Soc. Issues* **33**, 169-194.
Biewener, A. A. and Full, R. J. (1992). Force platform and kinematic analysis. In *Biomechanics–Structures and Systems: A Practical Approach* (ed. A. Biewener), pp. 45-73. Oxford: Oxford University Press.
Bobbert, M. F., Yeadon, M. R. and Nigg, B. M. (1992). Mechanical analysis of the landing phase in heel-toe running. *J. Biomech.* **25**, 223-234.
Croft, J. L. and Bertram, J. E. A. (2017). Affordance boundaries are defined by dynamic capabilities of Parkour athletes in dropping from various heights. *Front. Psychol.* **8**, 1571.
Croft, J. L., Schroeder, R. T. and Bertram, J. E. A. (2017). The goal of locomotion: Separating the fundamental task from the mechanisms that accomplish it. *Psychon. Bull. Rev.* **24**, 1675-1685.
Darici, O., Temeltas, H. and Kuo, A. D. (2018). Optimal regulation of bipedal walking speed despite an unexpected bump in the road. *PLoS ONE* **13**, e0204205.
Doke, J., Donelan, J. M. and Kuo, A. D. (2005). Mechanics and energetics of swinging the human leg. *J. Exp. Biol.* **208**, 439-445.
Donelan, J. M., Kram, R. and Kuo, A. D. (2002a). Mechanical work for step-to-step transitions is a major determinant of the metabolic cost of human walking. *J. Exp. Biol.* **205**, 3717-3727.
Donelan, J. M., Kram, R. and Kuo, A. D. (2002b). Simultaneous positive and negative external mechanical work in human walking. *J. Biomech.* **35**, 117-124.
Geyh, P. (2006). Urban free flow: a poetics of parkour. *M/C Journal*, **9**, 3. Retrieved from http://journal.media-culture.org.au/0607/06-geyh.php.
Gill, P. E., Murray, W. and Saunders, M. A. (2005). SNOPT: An SQP algorithm for large-scale constrained optimization. *SIAM* **47**, 99-131.
Hasaneini, S. J., Mcnab, C. J. B., Bertram, J. E. A. and Leung, H. (2013). The dynamic optimization approach to locomotion dynamics: human-like gaits from a minimally-constrained biped model. *Adv. Robot.* **27**, 845-859.
Hedrick, T. L. (2008). Software techniques for two- and three-dimensional kinematic measurements of biological and biomimetic systems. *Bioinspir. Biomim.* **3**, 034001.
Kennedy, S., Lee, D. V., Bertram, J. E. A., Lust, G., Williams, A. J., Soderholm, L. V., Hamilton, S., Bliss, S. P., Dykes, N. L., Todhunter, R. J. et al. (2003). Gait evaluation in hip osteoarthritic and normal dogs using a serial force plate system. *Vet. Comp. Orthop. Traumatol.* **16**, 170-177.
Lee, C. R. Farley, C. T. (1998). Determinants of the center of mass trajectory in human walking and running. *J. Exp. Biol.* **201**, 2935-2944.
Lee, D. V., Bertram, J. E. A. and Todhunter, R. J. (1999). Acceleration and balance in trotting dogs. *J. Exp. Biol.* **202**, 3565-3573.

Liu, W. and Nigg, B. M. (2000). A mechanical model to determine the influence of masses and mass distribution on the impact force during running. *J. Biomech.* **33**, 219-224.
Margaria, R. (1976). *Biomechanics and Energetics of Muscular Exercise*. Oxford, England: Clarendon Press.
Mauroy, G., Schepens, B. and Willems, P. A. (2013). The mechanics of running while approaching and jumping over an obstacle. *Eur. J. Appl. Physiol.* **113**, 1043-1057.
Mould, O. (2009). Parkour, the city, the event. *Environ. Plan. D* **27**, 738-750.
Patterson, M. A. and Rao, A. V. (2014). GPOPS-II: A MATLAB software for solving multiple-phase optimal control problems using hp-adaptive Gaussian quadrature collocation methods and sparse nonlinear programming. *ACM Trans. Math. Softw.* **41**, 1-37.
Polet, D. T., Schroeder, R. T. and Bertram, J. E. A. (2017). Reducing gravity takes the bounce out of running. *J. Exp. Biol.* **221**, 162024.
Puddle, D. L. and Maulder, P. S. (2013). Ground reaction forces and loading rates associated with parkour and traditional drop landing techniques. *J. Sports Sci. Med.* **12**, 122-129.
Ruina, A., Bertram, J. E. A. and Srinivason, M. (2005). A collisional model of the energetic cost of support work qualitatively explains leg sequencing in walking and galloping, pseudo-elastic leg behavior in running and the walk-to-run transition. *J. Theor. Biol.* **237**, 170-192.
Schroeder, R. T. and Bertram, J. E. A. (2018). Minimally actuated walking: Identifying core challenges to economical legged locomotion reveals novel solutions. *Front. Robot. AI* **5**, 58.
Srinivasan, M. (2011). Fifteen observations on the structure of energy-minimizing gaits in many simple biped models. *J. R Soc. Interface* **8**, 74-98.
Srinivasan, M. and Ruina, A. (2006). Computer optimization of a minimal biped model discovers walking and running. *Nature* **439**, 72-75.
Taylor, J. E. T., Witt, J. K. and Sugovic, M. (2011). When walls are no longer barriers: perception of wall height in parkour. *Perception* **40**, 757-760.
Xiang, Y., Arora, J. S. and Abdel-Malek, K. (2010). Physics-based modeling and simulation of human walking: a review of optimization-based and other approaches. *Struct. Multidiscipl. Optim.* **42**, 1-23.